Proceedings of the Seventh International Conference on
Railway Technology: Research, Development and Maintenance
Edited by: J. Pombo
Civil-Comp Conferences, Volume 15, Paper 3.11
Civil-Comp Press, Edinburgh, United Kingdom, 2026
ISSN: 2753-3239, doi: 10.4203/ccc.15.3.11

Experimental Validation of the Torque-Modulation-Based Method for Train-Borne Coefficient of Friction Measurement

G. Jayasree Krishnan, Z. Yang, J. Moraal and Z. Li

Section of Railway Engineering, Delft University of Technology, the Netherlands

Abstract

Train-borne measurements of the Coefficient of Friction (CoF) through wheel slip can induce wheel-rail interface damage, and indirect filtering methods exhibit limited universal applicability due to their dependence on parametric models. To overcome these limitations, a torque-modulation-based CoF measurement method has been proposed, in which small sinusoidal torque modulations are superimposed on wheelset torque, and the resulting phase difference between the applied torque and wheel angular velocity signals indicates the CoF at the wheel-rail interface in proximity to friction saturation. The concept has been tested and verified by multibody dynamics simulations, whereas experimental validation has not been reported in accessible literature. This study experimentally validated the torque-modulation method using the V-Track test rig in the lab conditions. Torque modulation was systematically performed on the V-Track at multiple operating points along the creep curve, from low-torque conditions to friction saturation. At each operating condition, the applied torque and wheel angular velocity were recorded over three modulation cycles. Detailed data-processing procedures for phase-difference extraction are presented. The test results demonstrate good repeatability of phase difference over cycles. The measured phase-difference behaviour shows good agreement with theoretical predictions and simulation trends, confirming the fundamental validity of the torque-modulation method for train-borne CoF measurements.

Keywords: torque-modulation, phase difference, coefficient of friction, experiment, V-Track, creep-curve.

1 Introduction

Wheel-rail friction is often characterised by the Coefficient of Friction (CoF). Maximum traction and braking forces experienced by trains depend on the product of the normal load at the wheel-rail contact and the CoF. Thus, the CoF directly influences acceleration and braking distances, which, in turn, affect inter-train distances and ultimately track capacity utilisation. The open nature of railway infrastructure may introduce significant uncertainties in the CoF value due to changes in surface roughness [1], rolling velocity [2], normal load [2], and third-body layers [3-5]. Consequently, railway operators often use conservative, constant CoF estimates (e.g., 0.15 for Dutch railways [6]) in scheduling calculations, potentially underestimating network capacity when the actual CoF is higher, and introducing safety risks [7] or service cancellations when the actual CoF is lower. Reliable measurement of the CoF is thus desirable for optimising railway operations and future implementation of Automatic Train Operations (ATO).

Laboratory measurements of CoF using twin-disc [3], V-track [8], pin-on-disc [9], pendulum [10] and full-scale roller rig [2] setups are essential in understanding friction phenomena, but they are either prone to scaling issues or fail to replicate real track conditions accurately, yielding poor real-world correlation of the measured CoF [4]. Field measurements of CoF are often conducted with hand-operated tribometers [11] at low speeds (<10 km/h) and require traffic interruptions. The measured CoF values may differ significantly from values experienced by in-service trains [12]. Train-borne CoF measurements overcome these limitations, potentially enabling continuous network-wide measurement.

Train-borne CoF measurement methods may be either direct or indirect. Direct methods measure the tri-axial (normal, lateral and longitudinal) wheel-rail contact forces to calculate the Coefficient of Adhesion (CoA), the ratio of the total tangential force and the normal load at the wheel-rail contact, which is bounded by the CoF. Friction saturation is induced by applying large braking torques, making the measured CoA equal the CoF [12]. However, these approaches can have detrimental effects on rail and wheel interfaces due to high sliding forces and creepages. Indirect methods estimate the CoF continuously using vehicle dynamics and contact force models, along with algorithms such as the Kalman filter [13]. However, the universal applicability and reliability of these models remain uncertain, and field validation studies are scarce.

To overcome the challenges of current CoF measurement methods, a torque-modulation-based [14] CoF measurement concept was proposed [15]. The concept involves superimposing a small sinusoidal modulation on wheel torque, which induces an oscillation in the wheelset angular velocity. The wheel-rail friction force acts as a damper, producing a phase difference between the modulated torque and the wheel angular velocity. This phase difference may indicate the CoF at the wheel-rail interface in proximity to but before friction saturation [15]. Although the proposed concept shows promise and viability in simulation environments, no experimental validation of the torque-modulation concept exists in the current literature, to the best of the authors' knowledge. This paper presents an experimental validation of the torque-modulation-based CoF measurement method using the V-Track test rig.

Torque-modulation was performed at different points along the creep curve, starting from zero torque until friction saturation and the corresponding phase differences between the torque and angular velocity responses were calculated. The behaviour of the phase difference was then compared to the trend predicted by the theoretical formulation.

2 Methods

2.1 Concept of Torque-modulation-based CoF Measurement

The basic concept and theoretical formulation underlying the torque-modulation-based CoF measurement method were detailed in [15]. Under steady state conditions where the rolling velocity, wheel moment of inertia, normal load, rolling radius and frequency of the applied modulated torque remain constant, and there is no lateral creepage, the phase difference between the wheel angular velocity and the applied modulated torque ϕ is related to the slope of the creep curve (i.e., the creep coefficient $\frac{dCoA}{d\xi_x}$) at the operating point as

$$tan(\phi) \propto \frac{1}{\frac{dCoA}{d\xi_x}} \quad (1)$$

Where CoA is the Coefficient of Adhesion at the operating point, and ξ_x is the longitudinal creepage at the operating point. At low values of the applied torque, the operating point lies in the "linear" portion of the creep curve, where the creep coefficient has a positive value. As the applied torque approaches friction saturation, the operating point moves towards the "non-linear" portion of the creep curve. Consequently, the creep coefficient approaches zero, leading to a rapid increase in the phase difference [15]. This rapid increase in phase difference can serve as an indicator of the onset of friction saturation in a CoF measurement system.

2.2 V-Track Test Rig

The experimental study was conducted using the V-Track test rig, which consists of a ring-track with a nominal diameter of 2 m on which two wheel assemblies can roll, as shown in Figure 1. The ring track consists of four arc-shaped rail pieces connected by joints, each covering 90 degrees. The rails are mounted on 100 equally spaced sleepers, with rail pads in between. Rubber pads below the sleepers simulate the stiffness and damping of the ballast layer. The wheel assembly (also shown in Figure 1) were mounted to a rigid steel frame that extends to the centre of the ring track and forms a platform that can be rotated by a motor, pulling the wheels along the ring track. A torque shaft was used to connect one wheel (i.e., the measuring wheel) to a second motor via two gearboxes.

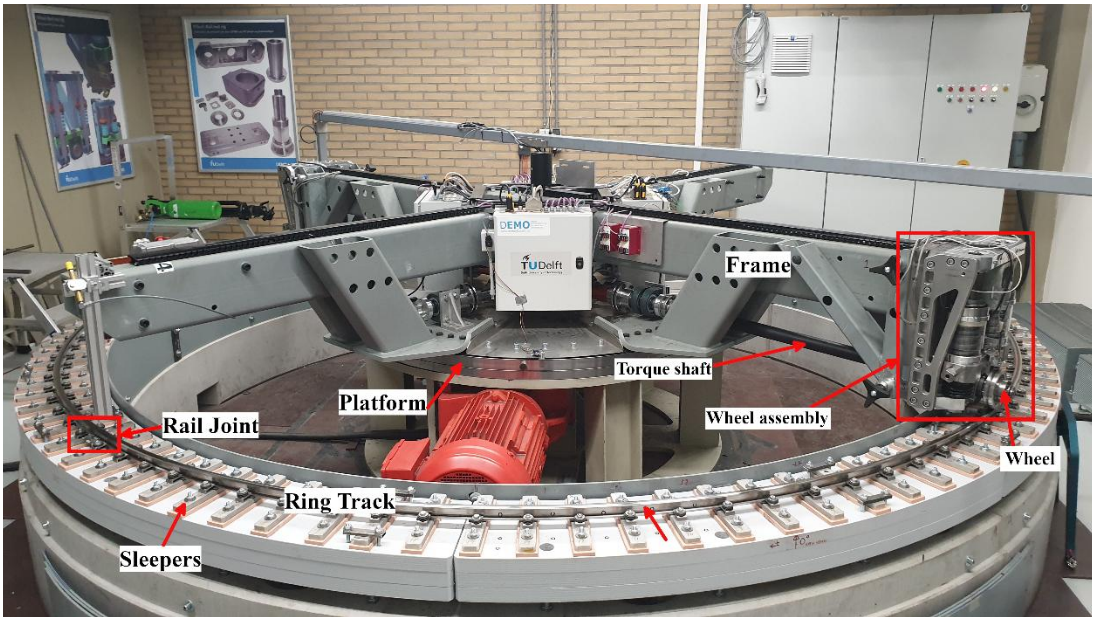

Figure 1: V-Track test rig.

The normal load on the wheel was set by adjusting two vertical springs which connect to the wheel via a guiding block and axle box. The guiding blocks enabled the wheels to move vertically, thus maintaining continuous contact with the ring track. Another motor was used to apply a prescribed traction torque, with or without modulation, to the wheel during rolling. A torque sensor with an integrated rotary encoder placed in-line with the torque shaft recorded the torque and angular velocity of the measuring wheel. A second rotary encoder positioned at the top of the frame measured the angular velocity of the platform. A four-sensor piezoelectric dynamometer system was placed between the wheel assembly and the steel frame to measure wheel-rail contact forces in three directions. A more detailed description of the design and measurement capabilities of the V-Track test rig can be found in [16] and [17], respectively.

2.3 Test Procedure

In the present study, the nominal wheel load was set at 4200 N, and the nominal rotational velocity of the platform was set at 7 km/h. The applied torque to the measuring wheel was calculated as the sum of two components: a DC component that provides the mean value of the torque signal and a sinusoidal modulation signal. The frequency and amplitude of the modulation signal were set at 2 Hz and 8 Nm, respectively. The DC torque was increased from zero in several steps till friction saturation. At each step, the applied torque, wheel angular velocity, platform angular velocity, and wheel-rail contact forces were recorded over three cycles, where each cycle represents the measuring wheel rolling a complete circle on the ring track. The DC torque was increased until slip occurred at the measuring wheel. A total of six torque steps were measured before slip, as shown in Table 1

Step no.	DC Applied Torque [Nm]
1	0.23
2	22.84
3	44.47
4	55.22
5	60.45
6	65.82

Table 1: Measured torque steps.

2.4 Data Processing

An example of the applied torque and wheel angular velocity recorded by V-Track for the third torque case is shown in Figure 2. Only one of the three recorded cycles is plotted to improve figure clarity.

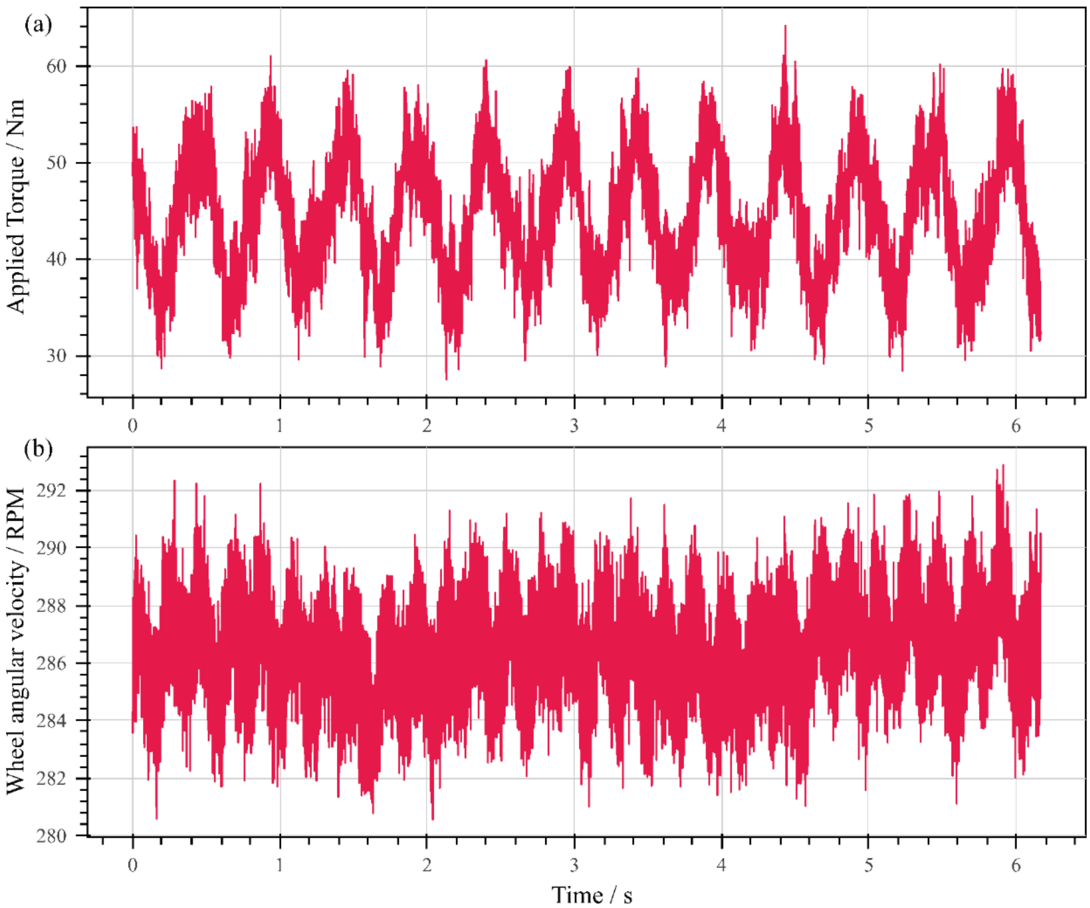

Figure 2: (a): Applied torque and (b): Wheel angular velocity signals recorded from V-Track.

The recorded signals contain contributions from vibration frequencies during the V-Track operation, which need to be filtered out so that we are left with the signal at the modulation frequency for calculating the phase difference. The data processing methodology followed these steps:

1. A Fast Fourier Transform (FFT) of the applied torque and wheel angular velocity was done to determine the actual modulation frequency. Table 2 presents the frequency with the highest amplitude within the search interval between 1.5 Hz and 2.5 Hz for torque and wheel angular speed in each recorded cycle. Although very close, there is a small difference in peak frequencies across cycles. To have a common modulation frequency, the average of the torque and wheel angular velocity peak frequencies for each cycle was considered as the common modulation frequency for that cycle, as shown in Table 2.

Cycle	Peak Frequency Torque [Hz]	Peak Frequency Wheel angular velocity [Hz]	Common modulation frequency [Hz]
1	2.0014	2.0111	2.00625
2	2.0029	2.0143	2.00860
3	2.0029	2.0159	2.00940

Table 2: Modulation frequencies from FFT and their average.

2. The data was recorded at a sampling frequency of 16670 Hz, which is too high compared to the modulation frequency. Thus, the data was first resampled to 53.344 Hz.
3. The wheel and platform angular velocity signals can be contaminated by eccentricity error of the respective measuring encoders [8], which needs to be filtered out. Two notch filters at the rotational frequency and its second harmonic were used to reduce the impact of encoder eccentricity.
4. A high-pass filter was then used to remove the DC component.
5. A band-pass filter of bandwidth 0.36 Hz, centred at the common modulation frequency (calculated in step 1), was used to filter out all other frequencies except the modulation frequency.
6. Because the motor controller uses its own internal clock to generate the sinusoidal signal to be applied to the wheel, the torque signals recorded for different cycles have different phases. To align the torques, the first recorded cycle was chosen as the reference. The unbiased cross-correlation of the torque signals from the second and third cycles relative to the first cycle was calculated using a maximum-lag window corresponding to one period of the modulation frequency. The lag that maximises the cross-correlation is the lag by which each cycle must be shifted to achieve the best alignment with the first cycle. The same lags were also used to shift the wheel angular velocity signals, such that the initial phase difference is unchanged.
7. For each pair of peak points (i.e., one from the applied torque and another from the wheel angular speed) and valley points, we can calculate a corresponding

phase difference (ϕ_{pair}, in degrees) from the time difference of the points (Δt_{pair}) in each pair by the relation

$$\phi_{pair} = 360 f_{mod} \Delta t_{pair} \tag{2}$$

where f_{mod} is the common modulation frequency. Since each modulation period has one peak and one valley, we have two phase differences per modulation period. These phase differences were calculated for three modulation cycles in the middle part of the signals because the beginning and end of the signals were distorted by filtering artefacts, and the cross-correlation function produces the best alignment near the centre of the signals. The average of all such calculated ϕ_{pair} for peak and valley points is the phase difference for that cycle.

8. To plot the creep curve, the longitudinal creepage was calculated using Equation (3):

$$\xi_x = \frac{\omega R_w - \Omega R_p}{\Omega R_p} \tag{3}$$

where Ω is the platform angular velocity, R_p is the platform radius (2.0 m), ω is the wheel angular velocity and R_w is the wheel radius. The CoA was obtained using Equation (4):

$$CoA = \frac{\sqrt{{F_x}^2 + {F_y}^2}}{F_z} \tag{4}$$

where F_x, F_y and F_z represent the measured wheel-rail contact forces in the longitudinal, lateral and normal directions. The mean values of the signals after notch filtering (i.e., after step 3) were used in the expressions of Equations (3) and (4).

9. The Polach model [18] was fitted onto the measured creep curve points using the least-squares approach. The velocity dependence of the CoF was not considered in the fitting because the rolling velocity was relatively low (7 km/h), and we measured only creep curve points before friction saturation at low creepage, whereas the velocity dependence of the CoF is prominent at high creepages due to temperature rise at the contact.

3 Results and Discussion

The creep curve measured at the torque steps in Table 1 is shown in Figure 3. The circular markers represent the pair of CoA and longitudinal creepage measured for each torque step. Vertical and horizontal error bars at each measurement point denote the variation in CoA and longitudinal creepage across repeated cycles at that point. The vertical error bar length corresponds to 20 times (to make the bars visible in the plot) the standard deviation of the measured CoA values, while the horizontal error bar length corresponds to five times the standard deviation of the measured creepage values. The dashed black line represents the fitted creep curve, using the Polach model. The fitted parameter value for the CoF is 0.24.

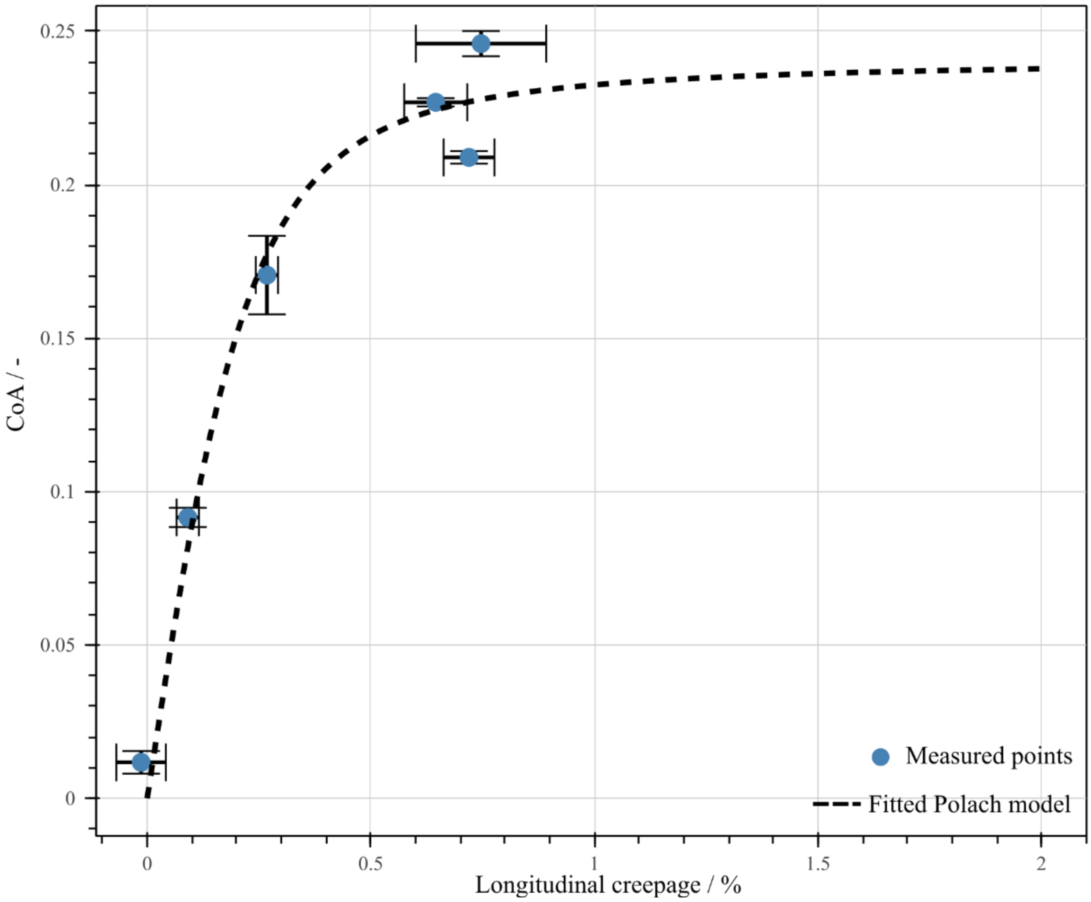

Figure 3: Measured creep curve along with the fitted Polach model.

The fitted creep curve is useful for qualitatively assessing the creep coefficient (i.e., the slope of the creep curve) at the measured points. From Figure 3, we observe that the creep coefficient remains relatively stable, with a positive value, for the first three measured points, but decreases sharply at the fourth measured point. This smaller creep coefficient is then approximately maintained for the fifth and sixth measured points.

The behaviour of the phase difference across the measured creep curve points is shown in Figure 4. The horizontal axis in Figure 4 is the applied DC torque at each measured point, represented as a percentage of the saturation torque. The saturation torque (T_s) was calculated as $T_s = \mu N R_w$ where the fitted parameter value for the CoF (0.24) was used. Vertical error bars at each point denote the variation in the calculated phase difference across repeated cycles. The vertical error bar length corresponds to the standard deviation of the calculated phase difference values.

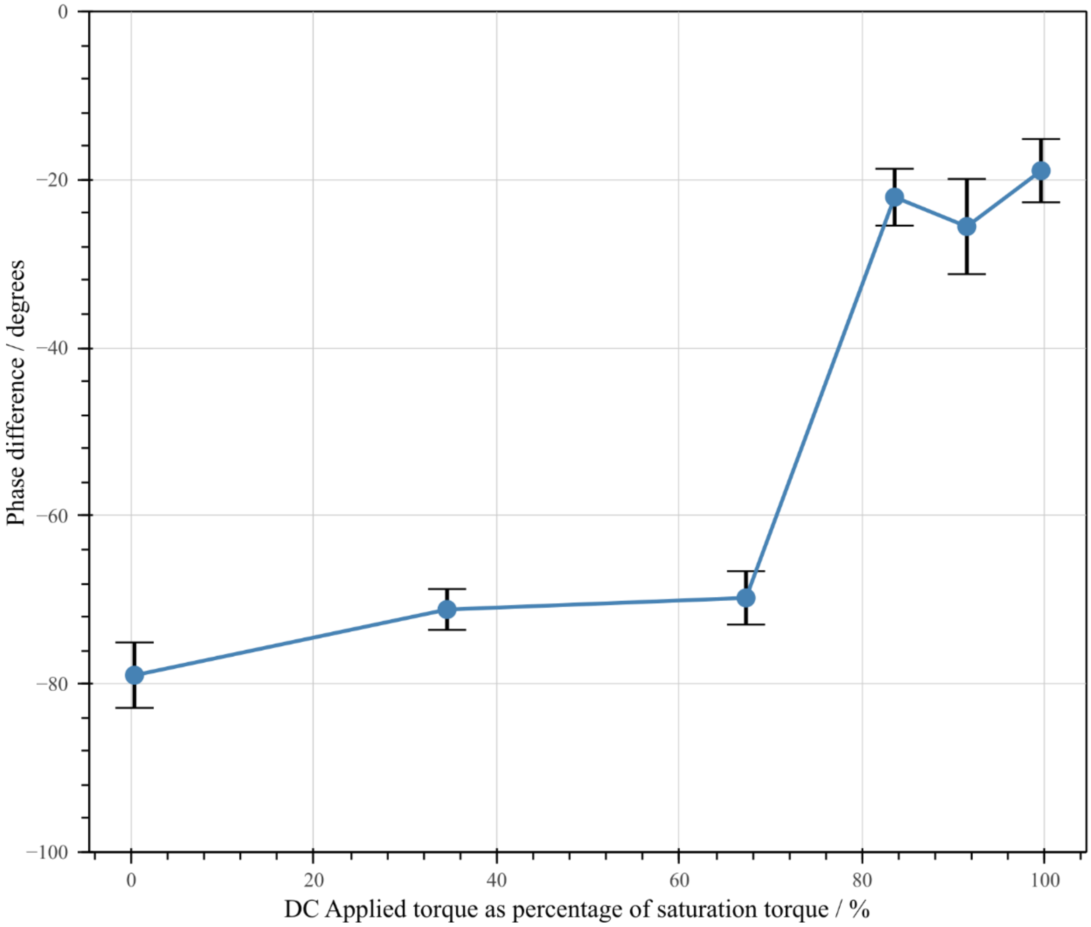

Figure 4: Measured phase difference progression with the applied torque DC level.

The short length of the error bars indicates good repeatability in the phase difference measurements. We observe from Figure 4 that the phase difference remains relatively constant for the first three measured points, then increases sharply at the fourth point, after which it remains relatively stable. This behaviour is in good agreement with the inverse relation between the creep coefficient and the phase difference predicted by Equation (1), and thus constitutes experimental validation of the torque-modulation method. Additionally, the overall trend of the phase difference, where it changes gradually at low torque and rapidly decreases when moving towards saturation, is broadly similar to the phase difference progression curve obtained in simulation environments [15].

4 Conclusions

This study provides initial experimental validation of the torque-modulation-based CoF measurement method using the V-Track test rig. In the V-Track test, the torque applied to the wheel was modulated with a small sinusoidal signal. The torque modulation was performed at different operating points along the creep curve, from low torque until friction saturation. At each point, the applied torque and wheel angular velocity were recorded for three cycles to guarantee repeatability. The data-processing steps used to obtain the phase difference were detailed. The results indicate good repeatability in phase difference at each measured point. The overall behaviour of the phase difference is in good agreement with the trend predicted by the theoretical formulations and with that obtained in simulations reported in the existing literature. Further research will focus on a more comprehensive validation of the torque-modulation-based CoF measurement method, e.g., by measuring the phase-difference progression curves under different CoF conditions (in the presence of water, friction modifiers, etc.) and then comparing with the theoretical formulations. Sensitivity studies to understand the dependence of the phase difference on modulation and operational parameters will also be conducted for practical implementations into the train-borne CoF measurements.

References

[1] Tanimoto, H., and Chen, H., 2015, "Influence of Surface Roughness and Temperature on Wheel / Rail Adhesion in Wet Conditions," Quarterly Report of RTRI, 56(3), pp. 206–211. https://doi.org/10.2219/rtriqr.56.206.

[2] Zhang, W., Chen, J., Wu, X., and Jin, X., 2002, "Wheel/Rail Adhesion and Analysis by Using Full Scale Roller Rig," Wear, 253(1-2), pp. 82–88. https://doi.org/10.1016/S0043-1648(02)00086-8.

[3] Li, Z., Arias-Cuevas, O., Lewis, R., and Gallardo-Hernández, E. A., 2009, "Rolling–Sliding Laboratory Tests of Friction Modifiers in Leaf Contaminated Wheel–Rail Contacts," Tribology Letters, 33(2), pp. 97–109. https://doi.org/10.1007/s11249-008-9393-3.

[4] Chang, C., Chen, B., Cai, Y., and Wang, J., 2019, "An Experimental Study of High Speed Wheel-Rail Adhesion Characteristics in Wet Condition on Full Scale Roller Rig," Wear, 440-441, p. 203092. https://doi.org/10.1016/j.wear.2019.203092.

[5] Wang, W. J., Zhang, H. F., Wang, H. Y., Liu, Q. Y., and Zhu, M. H., 2011, "Study on the Adhesion Behaviour of Wheel/Rail Under Oil, Water and Sanding Conditions," Wear, 271(9-10), pp. 2693–2698. https://doi.org/10.1016/j.wear.2010.12.019.

[6] Popovici, R. I., 2010, "Friction in Wheel-Rail Contacts," Ph.D., University of Twente.

[7] Gan, W., Wu, Y., Bai, Z., Hu, Y., Hou, Z., Li, X., and Chen, K., 2025, "Research and Application of Adhesion Optimization Control in the Traction System of Permanent Magnet High-Speed EMU Trains," Transportation Safety and Environment, 7(1), p. tdae025. https://doi.org/10.1093/tse/tdae025.

[8] Krishnan, G. J., Moraal, J., Li, Z., and Yang, Z., 2025, "An Experimental Study of Wheel–Rail Creep Curves Under Dry Contact Conditions Using V-Track," Lubricants, 13(7), p. 287. https://doi.org/10.3390/lubricants13070287.

[9] Olofsson, U., and Sundvall, K., 2004, "Influence of Leaf, Humidity and Applied Lubrication on Friction in the Wheel-Rail Contact: Pin-on-Disc Experiments," Proceedings of the Institution of Mechanical Engineers, Part F: Journal of Rail and Rapid Transit, 218(3), pp. 235–242. https://doi.org/10.1243/0954409042389364

[10] Lewis, S. R., Lewis, R., and Olofsson, U., 2011, “An Alternative Method for the Assessment of Railhead Traction,” Wear, 271(1-2), pp. 62–70. https://doi.org/10.1016/j.wear.2010.10.035.

[11] Harrison, H., 2008, “The Development of a Low Creep Regime, Hand-Operated Tribometer,” Wear, 265(9-10), pp. 1526–1531. https://doi.org/10.1016/j.wear.2008.03.028.

[12] Lundberg, J., Rantatalo, M., Wanhainen, C., and Casselgren, J., 2015, “Measurements of Friction Coefficients Between Rails Lubricated with a Friction Modifier and the Wheels of an IORE Locomotive During Real Working Conditions,” Wear, 324-325, pp. 109–117. https://doi.org/10.1016/j.wear.2014.12.002.

[13] Zhao, Y., Shen, Jiang, Zhang, Liu, Shu, and Peng, B., 2023, “Real-Time Wheel–Rail Friction Coefficient Estimation and Its Application,” Vehicle System Dynamics, 61(10), pp. 2598–2612. https://doi.org/10.1080/00423114.2022.2159846.

[14] Pichlík, P., 2020, “Summary of the Modern Wheel Slip Controller Principles,” TRANSACTIONS ON ELECTRICAL ENGINEERING, 8(2), pp. 26–31. https://doi.org/10.14311/TEE.2019.2.026.

[15] Krishnan, G. J., Yang, Z., Li, Z., and Dollevoet, R., 2025, “A Concept for Torque Modulation-Based Train-Borne Measurement of Coefficient of Friction,” Advances in Dynamics of Vehicles on Roads and Tracks III, W. Huang, and M. Ahmadian, eds., Springer Nature Switzerland, Cham, pp. 546–554. https://doi.org/10.1007/978-3-031-66971-2_57.

[16] Naeimi, M., Li, Z., Petrov, R. H., Sietsma, J., and Dollevoet, R., 2018, “Development of a New Downscale Setup for Wheel-Rail Contact Experiments Under Impact Loading Conditions,” Experimental Techniques, 42(1), pp. 1–17. https://doi.org/10.1007/s40799-017-0216-z.

[17] Zhang, P., Moraal, J., and Li, Z., 2021, “Design, Calibration and Validation of a Wheel-Rail Contact Force Measurement System in V-Track,” Measurement, 175, p. 109105. https://doi.org/10.1016/j.measurement.2021.109105.

[18] Polach, O. 2005, “Creep forces in simulations of traction vehicles running on adhesion limit”. Wear 258:992–1000 https://doi.org/10.1016/j.wear.2004.03.046